From 2D Design of Underactuated Bipedal Gaits to 3D Implementation: Walking with Speed Tracking

Xingye Da, Omar Harib, Ross Hartley, Brent Griffin and Jessy Grizzle

***Abstract*—Analysis and controller design methods abound in the literature for planar (aka 2D) bipedal models. This paper takes one of them developed for underactuated bipeds and documents the process of designing a family of controllers on the basis of a planar model and achieving stable walking on a physical 3D robot, both indoors and outdoors, with walking speed varying smoothly from 0 to 0.8 meters per second. The longest walk in a single experiment is 260 meters over terrain with ± 7 degrees of slope variation. Advantages and disadvantages of the design approach are discussed.**

I. Introduction

This paper focuses on taking a walking gait that has been designed and stabilized on the basis of an underactuated planar or 2D bipedal model, and implementing it on the 3D underactuated bipedal robot shown in Fig. 1. The lateral and sagittal planes of the robot are feedback controlled in a decoupled manner, while rotation in the transverse plane, hereafter referred to as yaw, is mechanically limited through narrow passive feet of non-zero length [16].

A large portion of the bipedal robotics literature considers planar models because they are simpler to understand, easier to analyze, and faster to simulate and optimize, to name just a few reasons. The authors of these papers, members of this paper's lab included, typically argue, imply or hope that insight or progress made on analysis and control methods for planar models serves as a valuable stepping stone to successful deployment on physical robots in 3D. The present paper will both support this line of thinking with analysis and experiments for at least one instance of a control design method, and offer words of caution where limitations of this approach are perceived.

A. Background

Research on passive bipedal walkers began with planar models [17, 31, 32]. It has been taken into the 3D realm in at least two ways. Kuo included roll dynamics with lateral hip actuation on an otherwise passive walker [28]. He showed that the open-loop system did not have stable limit cycles and then proposed a linear state variable feedback for the lateral dynamics to recover asymptotic stability when walking down shallow slopes. Collins et al. stabilized a truly passive walker in 3D through clever mechanical design of the feet [11], which coupled roll and yaw motions of the robot, though the domain of attraction of the limit cycle was impracticably small. The Cornell Ranger walked unsupported in 3D for 65 km [6]. Though the robot was powered, it used very minimal actuation in the sagittal plane and achieved passive (or mechanical) stabilization in the lateral plane through specially designed legs. A number of Wisse's robots have used passive means to achieve adequate lateral stabilization so that an essentially sagittal-plane robot could move about unsupported in 3D [12, 53, 54].

Moving to the other end of the actuation spectrum, fully actuated bipedal robots, Ames et al. developed a rigorous geometric framework to decouple the lateral and sagittal plane dynamics through functional Routhian Reduction[1] [3, 46, 47]. With this method, a controller derived from an appropriate planar model can provably create and stabilize a limit cycle in a 3D walker with yaw constrained to zero. The result was experimentally confirmed on NAO [4, 34], which achieved dynamically-stable forward walking at 15 cm/s. Gregg showed analysis and simulations of Routhian Reduction when yaw was un-actuated and viscous friction at the foot provided "rotational stabilization" [18, 19]. Kajita et al. first developed the linear inverted pendulum (LIP) model in 2D and demonstrated experimentally its application to bipedal walking [25]. The 2D and 3D LIP models proved fundamental in Pratt et al.'s work on capture point [27, 36]. Hosoda appears to implement decentralized sagittal and lateral control strategies on the pneumatically powered 3D biped Pneuman [23], though it is hard to be sure because the control algorithm is only partially described.

[1]This is related to reduction through conserved quantities, where, roughly speaking, the time rate of change of the momentum map evolves as a function of a cyclic variable.

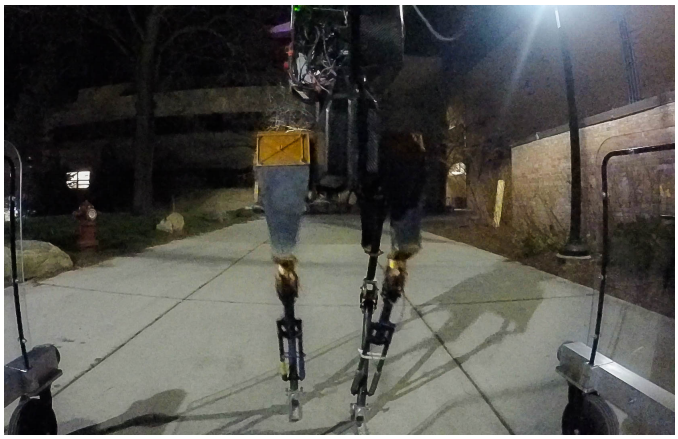

Fig. 1: Outdoor 3D walking with decoupled sagittal and lateral plane controllers [1, 2]. The ATRIAS-series robot is underactuated in pitch and roll, while yaw is mechanically constrained by passive feet.

In the middle of the actuation spectrum, hoppers were early examples of underactuated legged robots [38, 39]. Raibert developed the fundamental control strategy for Spring-Loaded Inverted Pendulum (SLIP) models and demonstrated that decoupled and identical sagittal and lateral plane controllers were adequate for control of his hoppers in 3D [38, 39]. Raibert's original SLIP-based strategy, perhaps augmented with foot placement [35, 37], has been extended to the family of robots created by Boston Dynamics [7]. Hurst designed the ATRIAS 2.1 series[2] of bipedal robots to instantiate approximately a 3D SLIP model [44]. The robot's legs are formed through a four-bar mechanism and series compliance actuation is implemented with leaf springs. The feet, when point-feet are not being used, are passive. Inspired by Raibert's SLIP-based controllers, Rezazadeh et al. designed decoupled lateral and sagittal plane controllers for ATRIAS [45], and demonstrated the robot's agility at the 2015 DRC [15]. The yaw motion of the robot was regulated passively through the feet shown in Fig. 2, which allow the leg end to act as a pivot with respect to pitch and roll, while yaw is limited through rubber pads attached to a narrow forward pointing bar that is approximately 20 cm in length.

B. Contributions and organization of this paper

This paper focuses on the process of designing a feedback controller on the basis of a planar bipedal model, and achieving a stable walking gait, both indoors and outdoors, on a 3D underactuated bipedal robot. Decoupled lateral and sagittal plane controllers will be used. The controller design builds upon previous work in [45, 9]. The primary contributions of the present paper include:

- A novel method is developed to continuously transition over a wide range of walking speeds. Relevant recent references are [51, 9], which designed gaits for a fixed forward speed.
- The sagittal controller design provides systematic and generalizable methods that consider the dynamic model and respect physical constraints commonly found in legged locomotion. The controller in [45, 15] was based on a SLIP model and hand tuning of parameters, which is limited to a specific class of robots.
- A means of unifying time- and phase-based controllers is presented.

The remainder of the paper is organized as follows. Section II describes the robot. A planar model of the robot is used in Section III to design a family of stabilized gaits, at speeds varying from walking in place to walking at 0.8 meter per second. A means to track a commanded speed profile is introduced. A simple controller to stabilize the lateral dynamics during straight-line walking is given in Section IV. Section V provides model-based analysis and simulation of the lateral and sagittal plane controllers on a 3D model of the robot. Section VI reports on experiments with the controller, both indoor and outdoors, while Sect. VII discusses advantages and disadvantages of the approach taken in the paper.

[2]ATRIAS stands for Assume the Robot Is A Sphere, emphasizing a 3D pendulum model.

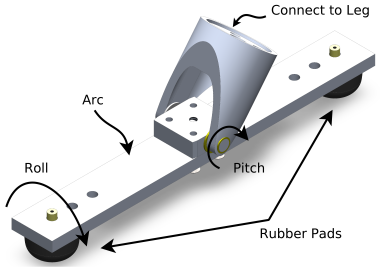

Fig. 2: A novel foot was introduced in [16]. Polyurethane rubber pads on the toe and heel reduce yaw, while leaving roll and pitch about the leg end free.

II. Mechanism Description

A. Robot Description

The bipedal robot shown in Fig. 1 and 3 is capable of 3D walking. Its total mass is 63 kg, with approximately 50% of the mass in the hips which house the four motor-harmonic drive assemblies for leg motion in the sagittal plane, and 40% of the mass in the torso, which houses the motors for the lateral motion of the legs and all of the electronics. The legs are very light and are formed by a four-bar linkage. The robot is approximately left-right symmetric. A more complete description is available in [40]

The configuration variables for the system can be defined as $q := (q_z, q_y, q_x, q_{1R}, q_{2R}, q_{3R}, q_{1L}, q_{2L}, q_{3L}) \in \mathbb{R}^9$. The variables (q_z, q_y, q_x) correspond to the world frame rotation angles, yaw, roll, and pitch. On the other hand, the variables $(q_{1R}, q_{2R}, q_{3R}, q_{1L}, q_{2L}, q_{3L})$ refer to local coordinates, seen in Fig. 3. These second set of coordinates are also actuated, giving us 6 degrees of actuation $u \in \mathbb{R}^6$ and 3 degrees of underactuation. It should be noted that the springs are assumed to be sufficiently stiff and have been deliberately neglected from the model. Also note that for control purposes, the leg coordinates (q_1, q_2) are rewritten as leg angle and knee angle (q_{LA}, q_{KA}), where $q_{LA} := \frac{1}{2}(q_1 + q_2)$ and $q_{KA} := q_2 - q_1$.

The actuators on the legs that drive the coordinates (q_1, q_2) each operate behind a 50:1 harmonic drive. For those motors, the power amplifiers allows the motors to generate torques up to 5 Nm as opposed to a maximum of 3 Nm, as was the case in previous work [9].

B. Yaw Reduction via Foot Design

The robot has been previously operated with a selection of different feet designs [8, 9]. In this work, the two-point-contact passive foot design of [16], shown in Fig. 2, has been adopted. The foot is composed of a revolute ankle that is connected to the leg (see Fig. 3(b)) and an arc that bridges two rubber pads. The ankle is free to rotate along a shaft on the arc, freeing the robot's pitch motion. In addition, the narrowness of the foot allows the robot to freely roll as well.

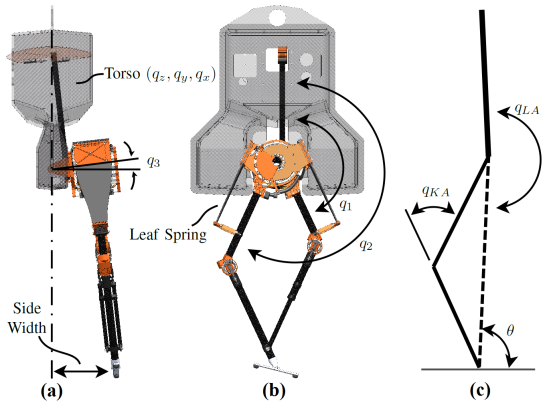

Fig. 3: Biped coordinates. (a) Lateral plane. (b) Sagittal plane. (c) Equivalent sagittal model.

As opposed to the "hoof" design used in [9], the 20 cm distance between the rubber contacts in the current foot counters yaw motion. Furthermore, in contrast to the prosthetic foot used in [8], which could initiate contact at the front or the back of the foot, the current foot acts like a point contact.

Ideally, with this foot in single support, the robot has two degrees of underactuation corresponding to pitch and roll. In practice, yaw is significantly reduced but not eliminated, as discussed in Section VI.

C. Models

The models used for controller design, analysis, and simulation were presented in [40]. In particular, the 2D representation is obtained from the 3D model by constraining $(q_y, q_z, q_{3L}, q_{3R})$ to zero. [40][Sec. 4.5].

III. 2D Gait Design and Stabilization

This section uses the 2D model to design an overall feedback controller that can walk in place, transition to, and maintain a desired walking speed, while employing walking gaits that are suitable for the conditions of the current step and respect mechanical constraints of the robot and environment. The basic walking controller is based on [52] and the walking in place controller is based on [45]. The optimization code used to generate walking gaits is based on [24]. The novel contribution lies in the methods for gait transition and speed regulation, which are achieved by inducing the longitudinal velocity of the robot to approximately evolve step to step as a discrete-time integrator, similar to that of an inverted pendulum, and then stabilizing the integrator with a simple foot placement algorithm. The controller is illustrated in Fig. 4.

A. Gait Design Using Virtual Constraints

Virtual constraints are kinematic relations among the generalized coordinates of the robot that are enforced asymptotically via continuous-time feedback control instead of by external forces. One virtual constraint in the form of a spline is imposed for each independent actuator in the planar model. Parameter optimization is used to select the coefficients in the virtual constraints so as to create a periodic orbit achieving a desired walking speed, while respecting physical constraints. Because the planar model has one degree of underactuation, when using the method of virtual constraints for controller design, local exponential stability of a periodic orbit of the closed-loop system can be established on the basis of a scalar quantity that can be directly included in the optimization process [52][pp. 130]. Several 2D robots [5, 10, 48, 56], and lower-limb prostheses have achieved walking and/or running using this approach [57]. See also [9, 43] for recent 3D results.

In the present paper, the collection of virtual constraints is expressed as an output vector

$$y = h_0(q) - h_d(s, \alpha), \tag{1}$$

to be asymptotically zeroed by a feedback controller. Here, $h_0(q)$ specifies the quantities to be controlled

$$h_0(q) = \begin{bmatrix} q_x \\ q^{st}_{KA} \\ q^{sw}_{LA} \\ q^{sw}_{KA} \end{bmatrix}, \tag{2}$$

where st and sw designate the stance and swing legs, respectively, and $h_d(s, \alpha)$ is a 4-vector of Beziér polynomials in the parameters α specifying the desired evolution of the $h_0(q)$.

When the desired walking speed of the periodic orbit is non-zero, the gait phasing variable, s, is defined as

$$s := \frac{\theta - \theta_{init}}{\theta_{final} - \theta_{init}} \in [0, 1], \tag{3}$$

where θ is the absolute stance leg angle defined in Fig. 3(c), θ_{init} is the initial value of θ each step, and θ_{final} is the final value of θ corresponding to the periodic orbit found in optimization. When the desired velocity is zero, or below a few tenths of a meter per second, time, normalized between zero and one, is used instead to parameterize the gait

$$\tau := \frac{t}{T} \in [0, 1], \tag{4}$$

where T is the duration of a step. In this case,

$$y = h_0(q) - h_d(\tau, \alpha). \tag{5}$$

In both cases, the optimization is performed as in [52] [Chp. 6.6.2], with the constraints given in Table I. Technically, when using (5), the model is augmented with

$$\dot{t} = 1, \tag{6}$$

and the zero dynamics are computed for the augmented model, and instead of integrating the squared torque and normalizing by step length [51][eq. (46)], the cost is taken as

$$J = \int_0^T ||u(t)||_2^2 dt, \tag{7}$$

with T fixed at 0.35 s [45]. Time-based gaits were designed for $-0.4 \leq v_{\text{sag}} \leq 0.2$ in increments of 0.2 m/s and phase-based gaits were designed for $0.4 \leq v_{\text{sag}} \leq 0.8$ with the same increments.

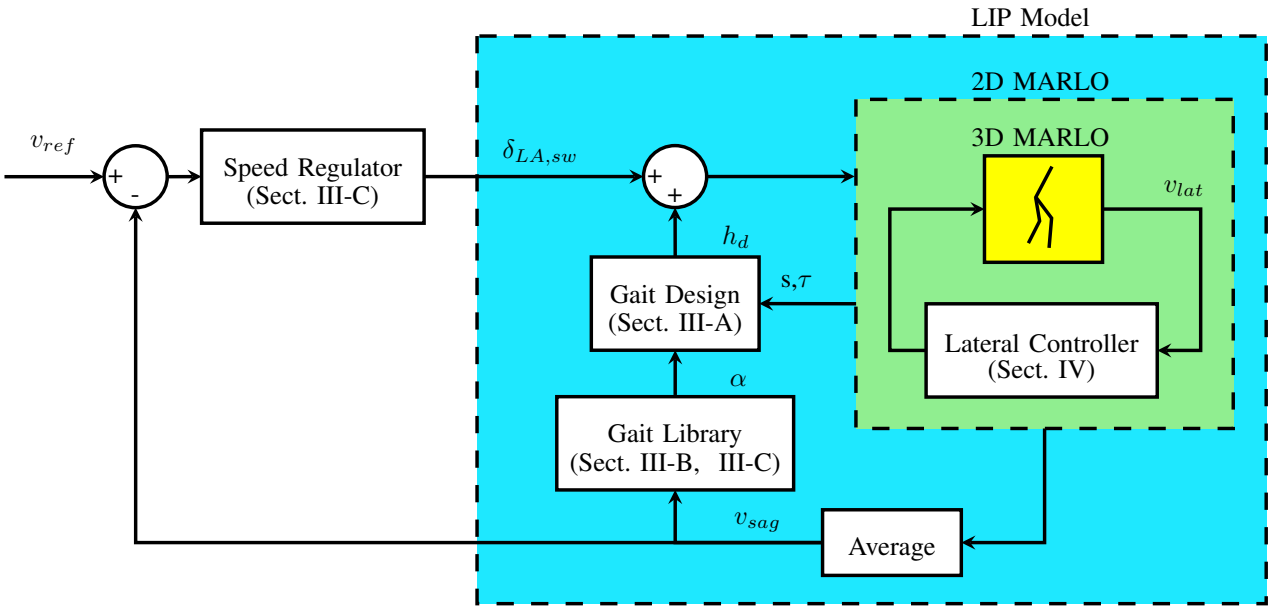

Fig. 4: Feedback diagram illustrating the control structure. The lateral controller is independent of the sagittal plane variables, making it possible to reduce the 3D model to 2D for sagittal controller design. Gait design implements virtual constraints in continuous time. Gait library updates gait parameters step to step based on the current speed, deliberately rendering the closed-loop system "approximately neutrally stable", analogous to an inverted pendulum (IP). The speed regulator works by adjusting swing foot leg angle.

TABLE I: Optimization constraints

Motor Toque $\|u\|$	< 5 Nm
Impact Impulse Fe	< 20 Ns
Friction Cone μ	< 0.4
Vertical Ground Reaction Force	> 300 N
Mid-step Swing Foot Clearance	> 0.15 m

B. Gait Library and Locally Stabilizing Feedback Controller

Four time-based gaits were designed for $-0.4 \leq v_{\text{sag}} \leq 0.2$ in increments of 0.2 m/s and four phase-based gaits were designed for $0.4 \leq v_{\text{sag}} \leq 1.0$ with the same increments, for a total of eight gait[3]. For values of v_{sag} between the discrete speeds, $v_{\text{sag,i}}, 1 \leq i \leq 8$, define the Beziér coefficients by linear interpolation

$$\zeta(v_{\text{sag}}) = \frac{v_{\text{sag}} - v_{\text{sag,i}}}{v_{\text{sag,i+1}} - v_{\text{sag,i}}}, \quad 1 \leq i \leq 7 \tag{8}$$

$$\alpha(v_{\text{sag}}) = (1 - \zeta(v_{\text{sag}}))\alpha_i + \zeta(v_{\text{sag}})\alpha_{i+1}. \tag{9}$$

The collection of gait designs is denoted by

$$\mathcal{A} = \{\alpha(v_{\text{sag}}) \mid -0.4 \leq v_{\text{sag}} \leq 1.0\}. \tag{10}$$

On the 2D and 3D models, as well as on the robot, the virtual constraints were implemented as in [51, Eqn. (47)] and [21] with a simple PD controller

$$u = -H^{-1}(K_p y + K_d \dot{y}), \tag{11}$$

[3]The number of gaits is arbitrary. A finer grid did not change the results. A coarser grid was not tried.

where

$$H = \begin{bmatrix} -1/2 & -1/2 & 0 & 0 \\ -1 & 1 & 0 & 0 \\ 0 & 0 & 1/2 & 1/2 \\ 0 & 0 & -1 & 1 \end{bmatrix}$$

is a constant matrix converting from control coordinates in (2) to the actuated coordinates. The gains K_p and K_d are the same for each gait.

C. Longitudinal Speed Regulation

The objective is to develop a novel speed controller with a broad basin of attraction. Tracking of a desired walking speed from zero to 0.8 m/s will be obtained. The design is done on the 2D model and then implemented on the 3D model.

Let $v_{\text{sag}}[k]$ be the average longitudinal speed of the robot at the middle of step k. The parameters of the virtual constraints (1) or (5) are updated to

$$\alpha[k] = \alpha(v_{\text{sag}}[k]). \tag{12}$$

This has two important consequences:

1) The local sagittal gait controller being applied is the one optimized for the current walking speed. Hence, the current controller respects the constraints enumerated in Table I. In particular, impact impulse, a key source of failure in experiments, should respect the designed constraints.
2) The closed-loop system is now "approximately neutrally" stable with respect to walking speed, similarly to an inverted pendulum or (IP) [25, 27, 36], or more

generally, what has been called a symmetric hybrid system (SHS) in [41, 42]. The equilibrium point of the closed-loop system now corresponds to $v_{\text{sag}}[k]$. If at the next step the robot's speed is perturbed by δv, under the update policy (12), the system's new equilibrium point will correspond to $v_{\text{sag}}[k+1] = v_{\text{sag}}[k] + \delta v$. This is similar to an integrator or a LIP model which have an eigenvalue exactly at one. Moreover, the eigenvalue of the closed-loop system that has been deliberately placed near one is independent of the current walking speed of the robot.

It is checked in Sec. V that this "re-centering" of the gait parameters about the current walking speed leaves all of the eigenvalues but one strictly within the unit circle. Hence, the advantages of the controllers designed above are maintained. Moreover, because of the approximate neutral stability of longitudinal speed step-to-step, a simple foot-placement controller can achieve speed regulation and tracking over a wide range of speeds with a constant set of controller gains.

The longitudinal speed regulator functions very similarly to the lateral controller in Sect. IV. Specifically, it sets a target offset in the swing leg angle

$$\begin{aligned}\delta^{sw}_{LA,tgt}[k] =& K_p\left(v_{\text{sag}}[k] - v^{\text{ref}}_{\text{sag}}\right) \\ &+ K_d\left(v_{\text{sag}}[k] - v_{\text{sag}}[k-1]\right), \end{aligned} \tag{13}$$

where $v^{\text{ref}}_{\text{sag}}$ is the reference speed. The offset can be implemented in many ways. When using virtual constraints, it can simply be added to the last value of the Beziér coefficients for the swing leg angle. Detailed virtual constraint based implementation could be seen in [34, 50].

D. Unifying The Timing Variable or Phase Used for Control

In (5), the links of the robot and its posture are being coordinated on the basis of time, while in (1) they are being coordinated with respect to an internal phase variable. Time- and phase-based parameterizations have relative advantages in different ranges of speed. When the robot is stepping in place for example, the phase variable (3) is not even well defined because θ_{init} and θ_{final}, the initial and final values of the mechanical phase variable, are approximately equal. In such a case, time is a more appropriate variable for synchronizing leg motion. When the robot is moving slowly, step length is very short and $\theta_{final} - \theta_{init}$ is only a few degrees, which may introduce too much sensitivity into the gait parametrization. On the other hand, extensive experimentation on Rabbit, Ernie [30], MABEL, and Amber [5] has shown the robustness of the phase-based implementations when walking at speeds exceeding several tenths of a meter per second. Gregg et al. are compiling evidence that human response to disturbances may actually better correlate with a mechanical phase variable than to time [20]. Kong et al. show that iterative learning control (ILC) performs better when trajectories are parameterized using phase rather than time [26].

The following is a means to combine time- and phase-based parameters into a single quantity. Let T be a nominal period of a gait and define

$$\dot{\tau} = \frac{1}{T} + \frac{L}{T}\left[s(q) - \tau\right], \quad \tau^+ = 0 \tag{14}$$

where $s(q)$ is computed as in (3) and $L \geq 0$ is a gain to be chosen. This can be viewed as a Luenberger observer for the phase. When $L = 0$, (14) reduces to (4), and a simple singular perturbation argument shows that as $L \to \infty$, (14) is purely phase-based. Here it is selected as

$$L(v_{\text{sag}}) = \begin{cases} 0 & |v_{\text{sag}}| < 0.4 \\ 7v_{\text{sag}} & \text{otherwise} \end{cases}, \tag{15}$$

which is sufficient to regard τ as "approximately" purely phase-based when $v_{\text{sag}} \geq 0.7$ m/s.

IV. Lateral Control for Straight-line Walking

While the design of the lateral controller is not a focus of this work, we provide in this section a simple lateral foot-placement strategy, based on [45], that is sufficient to extend 2D controllers to 3D for the robot in Fig. 1.

On a step-to-step basis, the objective is to obtain an asymptotically stable relationship

$$v_{\text{lat}}[k+1] = -k_1 v_{\text{lat}}[k] - k_0 v_{\text{lat}}[k-1], \tag{16}$$

where k is the current step index, $v_{\text{lat}}[\ell]$ is average lateral velocity at step ℓ, and k_1, k_0 are gains such that the roots of $\lambda^2 + k_1\lambda + k_0$ are in the unit circle. Foot placement is a common means of regulating velocity over the ensuing step through selection of the ground contact point of the inverted pendulum formed by the stance leg end and the center of mass. A simple strategy based on average lateral velocity has the benefit of working independently of sagittal control, potentially enabling a 3D walking platform to function for a set of 2D controllers, as illustrated in Fig. 4.

Following [45, Eqn. (5)], lateral foot placement is regulated by the target swing hip angle by

$$\begin{aligned} q^{sw}_{3,tgt}[k] =& q_{3,\text{nom}} + K_p\left(v_{\text{lat}}[k] - v^{\text{ref}}_{\text{lat}}\right) \\ &+ K_d\left(v_{\text{lat}}[k] - v_{\text{lat}}[k-1]\right), \end{aligned} \tag{17}$$

where $q_{3,\text{nom}}$ is the nominal hip angle. The gains K_p and K_d are tuned by hand. Because it is the contact point where the foot is placed that matters, as Kuo points out in [28], any continuous-time controller that achieves $q^{sw}_{3,tgt}[k]$ before ground contact should be sufficient to stabilize the lateral dynamics.

For normal forward walking and walking in place, $v^{\text{ref}}_{\text{lat}} = 0$, although a non-zero reference velocity can be used to achieve sideways walking.

Torso roll angle stabilization is achieved using stance hip actuation (see [45, Eqn. (10)]).

V. Model-based Analysis and Simulation

This section provides analytical and simulation support for the various components of the overall controller presented in Sects. III and IV.

TABLE II: Largest eigenvalue of various controllers

v (m/s)	0.3	0.5	0.7
2D VC	0.93	0.94	0.91
2D VC-SR	0.76	0.73	0.64
3D L-VC	0.91	1.12	1.14
3D L-VC-SR	0.86	0.82	0.81

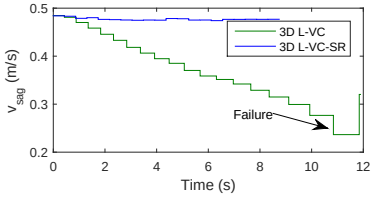

Fig. 5: Virtual constraints are designed for 0.5 m/s 2D walking and verified in 3D with the lateral controller. The controller (3D L-VC) slows down and fails, whereas the speed regulator (3D L-VC-SR) maintains the desired speed.

TABLE III: Three largest eigenvalues when $\alpha[k]$ is updated

v (m/s)	0.3	0.5	0.7
	1.04	0.98	1.09
2D VC-U	0.26	0.31	0.39
	0.19	0.20	0.25

A. Local exponential stability in 2D and 3D

The Poincaré map was used to check the existence of fixed points (i.e., periodic orbits) and to evaluate their stability. Table II first shows that the interpolated virtual constraint controllers (8), labeled (**2D VC**), at 0.3, 0.5 and 0.7 m/s induce local exponential stable fixed points in the 2D model, and that including the sagittal plane step length regulator (13), labeled (**2D VC-SR**), reduces the magnitude of the largest e-value. When implemented on the 3D model in combination with the lateral controller (17), stability is not always maintained for the virtual constraint controller, labeled (**3D L-VC**), while the inclusion of the step length regulator recovers local exponential stability; see (**3D L-VC-SR**). It is important to note that in this analysis, the parameters in the virtual constraints are being held constant step to step; they are not being updated as in (12).

Simulations of the (**3D L-VC**) and (**3D L-VC-SR**) controllers for 0.5 m/s are shown in Fig. 5. Without explicity speed regulation, the robot with (**3D L-VC**) slows to a point that it cannot complete a step and falls.

B. Parameter Update based on Longitudinal Speed

Table. III illustrates the "approximate neutral" stability of the planar controller, labeled (**2D VC-U**), when the gait parameters are updated step to step on the basis of longitudinal speed (12). It is seen that the largest eigenvalue is near one where others are significantly less than one.

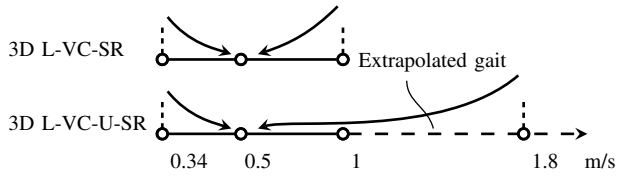

Fig. 6: Updating $\alpha[k]$ enhances ability to reject velocity perturbations.

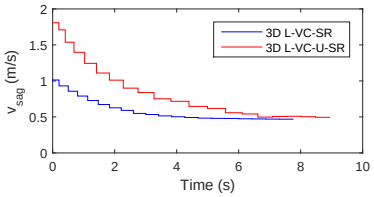

Fig. 7: Two controllers recovering to nominal speed 0.5 m/s from respective largest speed perturbation.

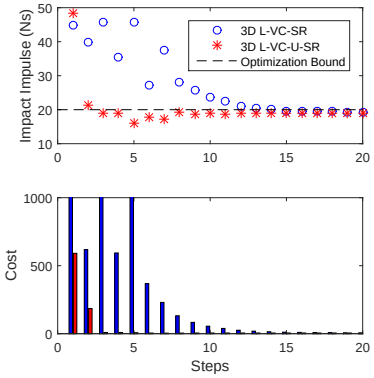

Fig. 8: (Top) Evolution of impact impulse optimization constraint with respect to step number when parameter updates are used versus not used. (Bottom) Associated cost function on the torques. Both simulations are initialized at 1 m/s and settle to the nominal speed of 0.5 m/s over 20 steps. Parameter updates significantly reduce the impulse during ground contact and the optimization cost (7).

Some of the benefits of performing the parameter updates are now illustrated. Figure 6 shows improved ability to handle longitudinal speed perturbations in 3D. When the controller parameters were initialized at $v_{\text{sag}} = 0.5$ m/s and held constant, the **3D L-VC-SR** controller can recover from an initial velocity of 1.0 m/s, but fails for larger speeds. On the other hand, when controller parameters were initialized at $v_{\text{sag}} = 0.5$ m/s and updated step to step, **3D L-VC-U-SR**, the simulated closed-loop could recover from an initial velocity of 1.8 m/s, considerably beyond the design range of the controller library[4]. A plot of speed versus time is shown in Fig. 7 over 20 steps of the gait.

A more important benefit is illustrated in Fig. 8, namely the reduction of the swing leg impact impulse[5] and a reduction

[4]Linear extrapolation was used to define the controller parameters.

[5]Related to swing leg vertical velocity at impact; see [33] for its correct definition.

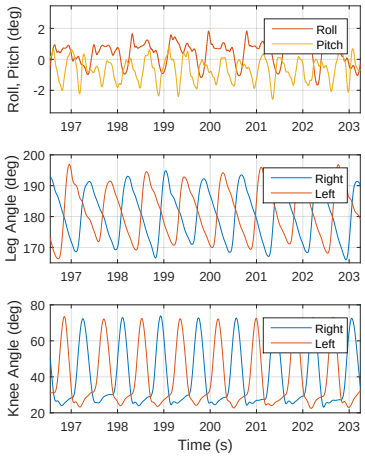

Fig. 9: Configuration variables changed during walking around 0.8 m/s. Roll was controlled to zero by lateral controller, while other variables were virtually constrained by sagittal controller.

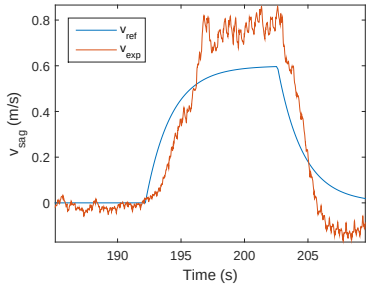

Fig. 10: Gait transition under complete controller. The robot transitions from zero to 0.8 m/s following the reference speed and then returns to walking in place.

in the cost (7). Very soon after the first parameter update takes place, the impact impulse constraint given in Table I is respected. On the other hand, without parameter updates, is only asymptotically respected.

VI. Experimental Results

This section illustrates several of the controllers on the physical 3D robot. Videos are available at [1, 2].

A. Partial Controller

The controller (**3D L-VC**) was executed five times on the robot, which was initialized at 0 m/s (i.e., walking in place), speed was increased to 0.4 m/s, and then the controller parameters were frozen at $v_{\text{sag}} = 0.6$ m/s. It fell quickly on four of the trials and achieved ten additional steps on one trial. This seems to support the analysis in Table. II.

When the speed regulator is added, the controller (**3D L-VC-SR**) produced consistent outcomes, with the robot always walking the full distance of the laboratory, approximately 10 m.

B. Complete Controller of Figure 4

The complete virtual constraint controller with updated gait parameters and speed regulator (**3D L-VC-U-SR**) is

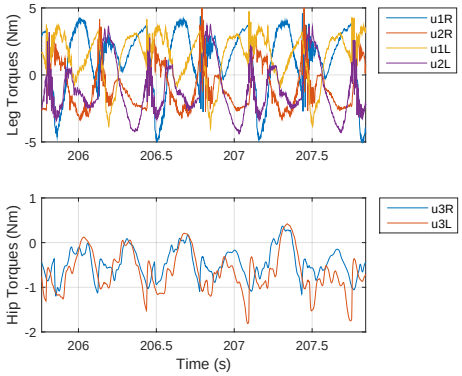

Fig. 11: Torque output of actuators on the motor side during walking in place. The leg motors are connected with a 50:1 gear box while the hip's gear ratio is 26.7:1

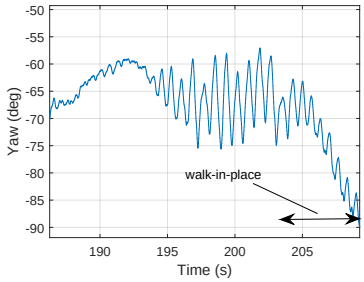

Fig. 12: Although the two-point-contact feet reduce the yaw motion, it is not fully eliminated. Yaw angle drifted about 20° while walking in place.

implemented on indoor and outdoor experiments. The controller achieves a top walking speed of approximately 0.8 m/s [1]. The longest walk in a single experiment is 260 meters with ±7 degrees of slope variation [2]. The posture of the robot, as reflected in the pitch and role angles of the torso, are consistently maintained as shown in Fig 9; in addition, it was consistent performance across multiple experiments. Compared to aforementioned partial controllers, the complete controller is able to transit seamlessly from 0 m/s to a target speed and then return to walking in place as shown in Fig. 10. To achieve this transition, **3D L-VC-U-SR** uses (14) and (15) to coordinate time- and phase-based control. Low speed walking uses time-based synchronization while walking speeds above 0.4 m/s transition to phase-based synchronization.

3D L-VC-U-SR is able to walk in place with lower torques than previous work with ATRIAS in [45] (see Fig. 11). Lower torques are the result of knees that are straighter and more rigid like the robot Rabbit [10], a torque-based optimization criterion (7), and constraints to avoid saturation (Table. I).

Fig. 12 shows yaw angle over a transition experiment. The feet successfully reduced yaw compared with previous work with ATRIAS in [9][Fig. 3], but yaw is not completely constrained. During walking in place, yaw drifts 20°.

VII. Discussion and Conclusions

This paper approached 3D walking by designing separate control modules for lateral stabilization, sagittal gait design,

and longitudinal speed regulation, as shown in Fig. 4. An advantage of this approach is that it gives a hierarchial view of control design. The lateral controller reduced the 3D model to 2D. Advanced control methods could be used efficiently in 2D to design a finite set of stabilizing controllers for a range of fixed walking speeds. In particular, the sagittal plane controllers were designed using a complete mechanical model of the robot, and this allowed important physical restrictions, such as actuator bounds, friction cone, contact impulse, and foot clearance to be directly addressed without hand-tuning on the robot. Interpolation and "re-centering" of the sagittal plane controllers allowed the construction of a continuous gait library of stabilizing controllers. When combined with a very simple speed regulator, this allowed the tracking of longitudinal speed commands, while continuing to respect important physical constraints even when walking speed varied.

This hierarchical method was shown to be effective on a physical robot by conducting experiments both in the laboratory and outdoors. The robot could be initialized to walk in place, and then commanded to increase speed to 0.8 m/s, followed by a reduction in speed to walking in place. For these experiments, yaw (or turning) was ignored in the control design. It was assumed instead that a yaw rate of approximately zero would be imposed passively through the foot design.

A clear advantage of using the full 2D model, versus replacing the robot immediately with one of the many pendulum models [25, 38, 39] when doing controller design, was that optimization could be employed, which provided a straightforward means to address the aforementioned physical constraints. A clear drawback of taking a decoupled perspective on the three primary planes of motion, sagittal, lateral, and transversal, is that it limits the type of gaits that can be achieved to those that do not "excite" inherent coupling in the dynamics. Agile motions such as rapid turning [49, 55] or dodging an obstacle clearly require using the full 3D model. For underactuated robots, however, even walking slowly in 3D is challenging because the periods of oscillation in the sagittal and lateral planes must be synchronized [42, 41, 25].

Counting on a physical means for yaw "stabilization" is a leap of faith at best, and a not uncommon means of failure in some of the experiments done on the robot used in this paper. Active steering is needed and will be added soon.

When walking in place, the mechanical phase variable used in previous work [52] was not a viable option, so time was used [43, 45]. A Luenberger-like estimator was used to combine time-based and phase-based gait controllers in a seamless manner. This needs to be analyzed more fully in future work.

The main effort of the laboratory has been, and will continue to be, dedicated to using the full 3-D model for gait and controller design for underactuated bipedal robots. Many of the advantages discussed for the 2D-gait library of Sect. III-B will carry over to the design of 3D controllers, with varying longitudinal, lateral, and rotational velocities. The size of the required libraries will grow. Recent optimization tools introduced in [22, 43] promise rapid 3D gait design with virtual constraints. In tandem with on-line planning algorithms [13, 14, 29], such controllers should lead to robots executing rapid dynamic maneuvers in 3D.

ACKNOWLEDGEMENT

Professor Jonathan Hurst (Oregon State University) and Mikhail Jones (Agility Robotics) are sincerely thanked for their advice on controller design for ATRIAS-series robots. The authors have also benefited greatly from discussions with PhD Student Hamed Razavi (Univ. of Michigan), Dr. Brian Buss (Ford Motor Company) and Prof. Kaveh Akbari Hamed (San Diego State University). The work in this paper is supported by the National Science Foundation through NSF grants ECCS-1343720 and ECCS-1231171.

REFERENCES

[1] Experiment Video: 2D Design to 3D Implementation. *https://youtu.be/ofMaxs09YQY*, December 2015.

[2] Experiment Video: Long Walk Outdoors. *https://youtu.be/eSllkIptlK0*, April 2016.

[3] A. D. Ames, R. D. Gregg, and M. W. Spong. A geometric approach to three-dimensional hipped bipedal robotic walking. In *45th Conference on Decision and Control*, San Diego, CA, 2007.

[4] A. D. Ames, E. A. Cousineau, and M. J. Powell. Dynamically stable robotic walking with NAO via human-inspired hybrid zero dynamics. In *Hybrid Systems, Computation and Control (HSCC)*, Philadelphia, April 2012.

[5] Aaron D Ames. Human-inspired control of bipedal walking robots. *Automatic Control, IEEE Transactions on*, 59(5):1115–1130, 2014.

[6] Pranav A Bhounsule, Jason Cortell, Anoop Grewal, Bram Hendriksen, JG Daniël Karssen, Chandana Paul, and Andy Ruina. Low-bandwidth reflex-based control for lower power walking: 65 km on a single battery charge. *The International Journal of Robotics Research*, 33(10): 1305–1321, 2014.

[7] Boston Dynamics. Atlas, The Next Generation. *https://www.youtube.com/watch?v=rVlhMGQgDkY*, April 2016.

[8] Brian G Buss, Alireza Ramezani, Kaveh Akbari Hamed, Brent A Griffin, Kevin S Galloway, and Jessy W Grizzle. Preliminary walking experiments with underactuated 3D bipedal robot marlo. In *Intelligent Robots and Systems (IROS 2014), 2014 IEEE/RSJ International Conference on*, pages 2529–2536. IEEE, 2014.

[9] Brian G Buss, Kaveh A Hamed, Brent A Griffin, and Jessy W Grizzle. Experimental results for 3D bipedal robot walking based on systematic optimization of virtual constraints. In *submitted to American Control Conference*, Boston, MA, June 2016.

[10] C. Chevallereau, G. Abba, Y. Aoustin, F. Plestan, E. R. Westervelt, C. Canudas, and J. W. Grizzle. RABBIT:

a testbed for advanced control theory. *IEEE Control Systems Magazine*, 23(5):57–79, October 2003.

[11] S. H. Collins, M. Wisse, and A. Ruina. A three-dimensional passive-dynamic walking robot with two legs and knees. *International Journal of Robotics Research*, 20(7):607–615, July 2001.

[12] S. H. Collins, A. Ruina, R. Tedrake, and M. Wisse. Efficient bipedal robots based on passive-dynamic walkers. *Science*, 307:1082–85, 2005.

[13] Robin Deits and Russ Tedrake. Efficient mixed-integer planning for uavs in cluttered environments. In *Robotics and Automation (ICRA), 2015 IEEE International Conference on*, 2015.

[14] Robin Deits and Russ Tedrake. Computing large convex regions of obstacle-free space through semidefinite programming. In *Algorithmic Foundations of Robotics XI*, pages 109–124. Springer, 2015.

[15] Dynamic Robotics Laboratory. ATRIAS: An Agile and Efficient Bipedal Robot. *https://www.youtube.com/watch?v=YFEJvb8iM7A*, April 2015.

[16] Dynamic Robotics Laboratory. ATRIAS Robot: First 3D Test. *https://www.youtube.com/watch?v=vq4Xq4eSCv8*, Feb 2015.

[17] A. Goswami, B. Espiau, and A. Keramane. Limit cycles in a passive compass gait biped and passivity-mimicking control laws. *Autonomous Robots*, 4(3):273–86, 1997.

[18] Robert D Gregg. Controlled reduction of a five-link 3D biped with unactuated yaw. In *Decision and Control and European Control Conference (CDC-ECC), 2011 50th IEEE Conference on*, pages 669–674. IEEE, 2011.

[19] Robert D Gregg and Ludovic Righetti. Controlled reduction with unactuated cyclic variables: Application to 3d bipedal walking with passive yaw rotation. *Automatic Control, IEEE Transactions on*, 58(10):2679–2685, 2013.

[20] Robert D Gregg, Elliott J Rouse, Levi J Hargrove, and Jonathon W Sensinger. Evidence for a time-invariant phase variable in human ankle control. *PloS one*, 9(2): e89163, 2014.

[21] J.W. Grizzle, Jonathan Hurst, B. Morris, Hae-Won Park, and K. Sreenath. MABEL, a new robotic bipedal walker and runner. In *American Control Conference, 2009. ACC '09.*, pages 2030–2036, 2009. doi: 10.1109/ACC.2009.5160550.

[22] Ayonga Hereid, Eric A Cousineau, Christian M Hubicki, and Aaron D Ames. 3D dynamic walking with underactuated humanoid robots: A direct collocation framework for optimizing hybrid zero dynamics. *Accepted in Robotics and Automation (ICRA), 2016 IEEE International Conference on*, 2016.

[23] Koh Hosoda, Takashi Takuma, and Masayuki Ishikawa. Design and control of a 3D biped robot actuated by antagonistic pairs of pneumatic muscles. In *Proceedings of International Symposium on Adaptive Motion in Animals and Machines*, 2005.

[24] Mikhail S Jones. Optimal control of an underactuated bipedal robot. 2014.

[25] S. Kajita, T. Yamaura, and A. Kobayashi. Dynamic walking control of biped robot along a potential energy conserving orbit. *IEEE Transactions on Robotics and Automation*, 8(4):431–37, August 1992.

[26] Felix H Kong, A Mounir Boudali, and Ian R Manchester. Phase-indexed ilc for control of underactuated walking robots. In *Control Applications (CCA), 2015 IEEE Conference on*, pages 1467–1472. IEEE, 2015.

[27] T. Koolen, T. de Boer, J. Rebula, A. Goswami, and J. Pratt. Capturability-based analysis and control of legged locomotion, Part 1: Theory and application to three simple gait models. *The International Journal of Robotics Research*, (9):1094–1113, July . ISSN 0278-3649. doi: 10.1177/0278364912452673.

[28] A. D. Kuo. Stabilization of lateral motion in passive dynamic walking. *International Journal of Robotics Research*, 18(9):917–930, 1999.

[29] Ian R Manchester and Jack Umenberger. Real-time planning with primitives for dynamic walking over uneven terrain. In *Robotics and Automation (ICRA), 2014 IEEE International Conference on*, pages 4639–4646. IEEE, 2014.

[30] Anne E Martin, David C Post, and James P Schmiedeler. Design and experimental implementation of a hybrid zero dynamics-based controller for planar bipeds with curved feet. *The International Journal of Robotics Research*, 33 (7):988–1005, 2014.

[31] T. McGeer. Passive dynamic walking. *International Journal of Robotics Research*, 9(2):62–82, April 1990.

[32] T. McGeer. Passive walking with knees. In *Proc. of the 1990 IEEE International Conference on Robotics and Automation, Cincinnati, OH*, volume 3, pages 1640–1645, May 1990. doi: 10.1109/ROBOT.1990.126245.

[33] Hae-Won Park, K. Sreenath, J. W. Hurst, and J. W. Grizzle. Identification of a bipedal robot with a compliant drivetrain. *IEEE Control Systems Magazine*, 31(2):63 – 88, april 2011. ISSN 1066-033X. doi: 10.1109/MCS.2010.939963.

[34] Matthew J Powell, Ayonga Hereid, and Aaron D Ames. Speed regulation in 3D robotic walking through motion transitions between human-inspired partial hybrid zero dynamics. In *Robotics and Automation (ICRA), 2013 IEEE International Conference on*, pages 4803–4810. IEEE, 2013.

[35] J. Pratt and R. Tedrake. Velocity-based stability margins for fast bipedal walking. In Moritz Diehl and Katja Mombaur, editors, *Fast Motions in Biomechanics and Robotics*, volume 340 of *Lecture Notes in Control and Information Sciences*, pages 299–324. Springer Berlin Heidelberg, 2006. ISBN 978-3-540-36118-3. doi: 10.1007/978-3-540-36119-0_14.

[36] J. Pratt, T. Koolen, T. de Boer, J. Rebula, S. Cotton, J. Carff, M. Johnson, and P. Neuhaus. Capturability-based analysis and control of legged locomotion, Part 2: Application to M2V2, a lower-body humanoid. *The International Journal of Robotics Research*, (10):1117–

1133, August . ISSN 0278-3649. doi: 10.1177/0278364912452762.

[37] J. Pratt, J. Carff, S. Drakunov, and A. Goswami. Capture Point: A Step toward Humanoid Push Recovery. *2006 6th IEEE-RAS International Conference on Humanoid Robots*, 2006. doi: 10.1109/ICHR.2006.321385.

[38] M. H. Raibert. *Legged robots that balance*. MIT Press, Mass., 1986.

[39] M. H. Raibert. Legged robots. *Communications of the ACM*, 29(6):499–514, 1986.

[40] Alireza Ramezani, Jonathan W. Hurst, Kaveh Akbari Hamed, and J. W. Grizzle. Performance Analysis and Feedback Control of ATRIAS, A Three-Dimensional Bipedal Robot. *Journal of Dynamic Systems, Measurement, and Control*, 136(2), 2014.

[41] Hamed Razavi, Anthony M Bloch, Christine Chevallereau, and Jessy W Grizzle. Symmetry in 3D Legged Locomotion: A New Method for Designing Stable Periodic Gaits. *Submitted to Autonomous Robots*, 2015.

[42] Hamed Razavi, Anthony M. Bloch, Chevallereau Christine, and Jessy W. Grizzle. Restricted discrete invariance and self-synchronization for stable walking of bipedal robots. In *Proceedings of the American Control Conference*, July 2015.

[43] Jacob Reher, Eric Cousineau, Ayonga Hereid, Christian M Hubicki, and Aaron D Ames. Realizing dynamic and efficient bipedal locomotion on the humanoid robot DURUS. *Accepted in Robotics and Automation (ICRA), 2016 IEEE International Conference on*, 2016.

[44] Daniel Renjewski, Alexander Sprowitz, Andrew Peekema, Mikhail Jones, and Jonathan Hurst. Exciting engineered passive dynamics in a bipedal robot. *Robotics, IEEE Transactions on*, 31(5):1244–1251, 2015.

[45] Siavash Rezazadeh, Christian Hubicki, Mikhail Jones, Andrew Peekema, Johnathan Van Why, Andy Abate, and Jonathan W Hurst. Spring-mass walking with atrias in 3D: Robust gait control spanning zero to 4.3 kph on a heavily underactuated bipedal robot. *ASME Dynamic Systems and Control Conference (DSCC)*, page 23, 2015.

[46] R. W. Sinnet and A. D. Ames. 2D bipedal walking with knees and feet: A hybrid control approach. In *48th IEEE Conference on Decision and Control*, Shanghai, P.R. China, 2009.

[47] R. W. Sinnet and A. D. Ames. 3D bipedal walking with knees and feet: A hybrid geometric approach. In *48th IEEE Conference on Decision and Control*, Shanghai, P.R. China, 2009.

[48] Koushil Sreenath, Hae-Won Park, Ioannis Poulakakis, and JW Grizzle. Embedding active force control within the compliant hybrid zero dynamics to achieve stable, fast running on mabel. *The International Journal of Robotics Research*, 32(3):324–345, 2013.

[49] Patrick M Wensing and David Orin. 3D-slip steering for high-speed humanoid turns. In *Intelligent Robots and Systems (IROS 2014), 2014 IEEE/RSJ International Conference on*, pages 4008–4013. IEEE, 2014.

[50] E. R. Westervelt, J. W. Grizzle, and C. Canudas. Switching and PI control of walking motions of planar biped walkers. *IEEE Transactions on Automatic Control*, 48 (2):308–12, February 2003.

[51] E. R. Westervelt, G. Buche, and J. W. Grizzle. Experimental validation of a framework for the design of controllers that induce stable walking in planar bipeds. *International Journal of Robotics Research*, 23(6):559–82, 2004.

[52] E. R. Westervelt, J. W. Grizzle, C. Chevallereau, J. H. Choi, and B. Morris. *Feedback Control of Dynamic Bipedal Robot Locomotion*. Control and Automation. CRC Press, Boca Raton, FL, June 2007.

[53] Martijn Wisse. Three additions to passive dynamic walking: actuation, an upper body, and 3D stability. *International Journal of Humanoid Robotics*, 2(04):459–478, 2005.

[54] Martijn Wisse, Arend L Schwab, and RQ vd Linde. A 3D passive dynamic biped with yaw and roll compensation. *Robotica*, 19(03):275–284, 2001.

[55] Aimin Wu and Hartmut Geyer. The 3-D spring–mass model reveals a time-based deadbeat control for highly robust running and steering in uncertain environments. *Robotics, IEEE Transactions on*, 29(5):1114–1124, 2013.

[56] T Yang, ER Westervelt, A Serrani, and James P Schmiedeler. A framework for the control of stable aperiodic walking in underactuated planar bipeds. *Autonomous Robots*, 27(3):277–290, 2009.

[57] Huihua Zhao, Jake Reher, Jonathan Horn, Victor Paredes, and Aaron D Ames. Demonstration of locomotion with the powered prosthesis AMPRO utilizing online optimization-based control. In *Proceedings of the 18th International Conference on Hybrid Systems: Computation and Control*, pages 305–306. ACM, 2015.